CHEMISTRY
A EUROPEAN JOURNAL

DOI: 10.1002/chem.200801364

Interaction of Dinuclear Ruthenium(II) Supramolecular Cylinders with DNA: Sequence-Specific Binding, Unwinding, and Photocleavage

Jaroslav Malina,[a] Michael J. Hannon,[b] and Viktor Brabec*[a]

Abstract: Metallosupramolecular chemistry was used to design a new class of synthetic agents, namely, tetracationic supramolecular cylinders, that bind strongly and noncovalently in the major groove of DNA. To gain additional information on interactions of the cylinders with DNA we explored DNA unwinding and sequence-specific binding properties, as well as DNA photonuclease activity of ruthenium(II) metallosupramolecular cylinder $[Ru_2L_3]^{4+}$, where L is a bis-pyridylimine ligand. We found that $[Ru_2L_3]^{4+}$ unwinds negatively supercoiled plasmid DNA and exhibits binding preference to regular alternating purine–pyrimidine sequences in a similar way to the $[Fe_2L_3]^{4+}$ analogue. Photocleavage studies showed that, unlike $[Fe_2L_3]^{4+}$, $[Ru_2L_3]^{4+}$ induces single-strand breaks on irradiation by visible and UVA light and cleaves DNA mainly at guanine residues contained preferentially in regularly alternating purine–pyrimidine nucleotides. As $[Ru_2L_3]^{4+}$ binds and cleaves DNA in a sequence-dependent manner, it may provide a useful tool for basic and applied biology, such as for controlled manipulation of the genome.

Keywords: DNA cleavage · DNA unwinding · helical structures · ruthenium · supramolecular chemistry

Introduction

Since DNA encodes and regulates most aspects of life it represents a very important potential drug target. The design of agents that can bind and react in a sequence-specific manner with DNA is of a great importance in probing biological processes and in developing therapeutic drugs. In this field, ruthenium complexes have attracted particular interest.[1–5] In accordance with their chirality and photophysical and photoredox properties, they offer many possibilities for use in biochemical applications such as chiral or luminescent DNA probes, chemical photonucleases, and DNA photoreagents. A number of ruthenium compounds have attracted interest as new metal-based antitumor drugs, and two of them—NAMI-A and KP1019—have reached clinical trials. Most of the studied complexes can undergo coordinative binding to biomolecules, and a few are coordinatively saturated yet display some anticancer activity mediated by noncovalent biomolecule binding.

Recently, metallosupramolecular chemistry has been used to design a new class of synthetic agents, namely, tetracationic supramolecular cylinders, that bind strongly and noncovalently in the major groove of DNA and cause remarkable intramolecular coiling of DNA.[6–8] In these cylinders, for example, $[Fe^{II}_2L_3]^{4+}$ (Figure 1a and b), three bis-pyridylimine ligand strands are wrapped in a helical fashion about two metal centers, and face–edge π–π and metal–ligand interactions contribute to the structural rigidity of the unit.

Efforts to combine the striking DNA-binding features of metallosupramolecular cylinders with the photoactive properties of ruthenium recently came to fruition, and a new diruthenium triple-stranded cylinder based on the design of the previous iron cylinder $[Fe_2L_3]^{4+}$ was prepared.[9,10] X-ray crystallography demonstrated that the structure of $[Ru_2L_3]^{4+}$ (Figure 1a and c) is analogous to that of the corresponding iron(II) cylinder. Fluorescence, CD, and LD studies[10] showed that $[Ru_2L_3]^{4+}$ binds and coils DNA. In addition, the high stability of this compound, due to the inert ruthenium(II) centers, makes this type of agent particularly suitable for use in biological studies and perhaps as chemotherapeutics. It exhibits cytotoxic activity against human breast

[a] Dr. J. Malina, Prof. Dr. V. Brabec
Institute of Biophysics
Academy of Sciences of the Czech Republic, v.v.i.
Kralovopolska 135, 61265 Brno (Czech Republic)
Fax: (+420) 541-240-499
E-mail: brabec@ibp.cz

[b] Prof. Dr. M. J. Hannon
School of Chemistry, University of Birmingham
Edgbaston, Birmingham B15 2TT (UK)

Supporting information for this article is available on the WWW under http://dx.doi.org/10.1002/chem.200801364.

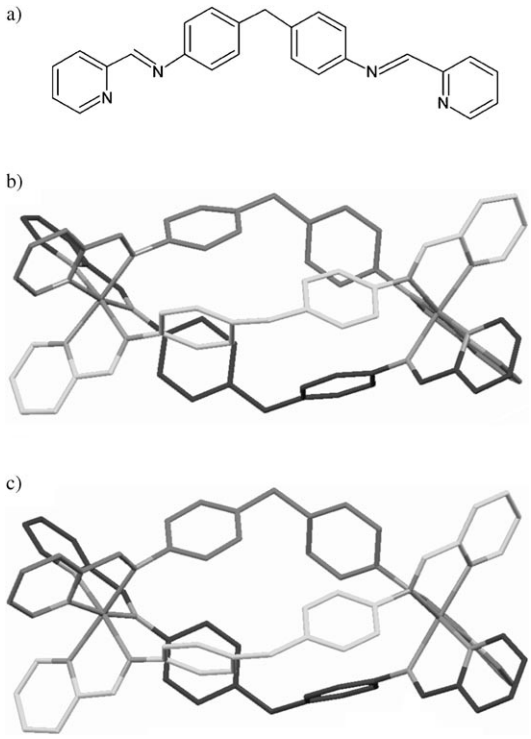

Figure 1. a) Ligand L in metallosupramolecular cylinders $[Fe_2L_3]^{4+}$ and $[Ru_2L_3]^{4+}$. Structures of cylinders $[Fe_2L_3]^{4+}$ (b) and $[Ru_2L_3]^{4+}$ (c) determined by X-ray crystallography.[10,24,25]

cancer cells HBL-100 and T47D,[10] which classifies it as a member of a new and promising group of noncovalent DNA-binding anticancer metallodrugs. A key goal of developing ruthenium cylinders was to harness the potential photochemical properties of ruthenium diimine centers within the cylinders. Herein we show that these agents have DNA photocleavage properties and that this can be used for DNA footprinting. Together with DNA unwinding assays we use this cylinder footprinting and competitive deoxyribonuclease I (DNase I) footprinting studies to probe DNA recognition and specificity of these cylinders. The results reveal that $[Ru_2L_3]^{4+}$ unwinds negatively supercoiled plasmid DNA and preferentially binds to regular alternating purine–pyrimidine sequences in a similar way to $[Fe_2L_3]^{4+}$.[11] Photocleavage studies show that, unlike $[Fe_2L_3]^{4+}$, $[Ru_2L_3]^{4+}$ induces single-strand breaks on irradiation by visible and UVA light and cleaves DNA mainly at guanine residues by generating singlet oxygen.

Results

Ethidium bromide displacement: The binding strength of $[Ru_2L_3]^{4+}$ to calf thymus (ct) DNA was quantified by means of the competition between cylinders and ethidium bromide (EtBr), as in our previous work.[11] Displacement of EtBr from all studied DNAs was accompanied by a decrease in the fluorescence intensity measured at 595 nm. The apparent binding constant K_{app} for $[Ru_2L_3]^{4+}$ binding to ct DNA, calculated as described in the Experimental Section, was $5.8\times10^7\,\text{M}^{-1}$. Thus, this competitive binding study shows that $[Ru_2L_3]^{4+}$ has a binding affinity for ct DNA similar to that of $[Fe_2L_3]^{4+}$.[11]

Unwinding of negatively supercoiled DNA: Local unwinding is a pronounced conformational alteration induced in DNA by $[Fe_2L_3]^{4+}$.[11] Hence, it was of interest to examine induction of DNA unwinding by its ruthenium counterpart and compare it with DNA unwinding by $[Fe_2L_3]^{4+}$. Figure 2

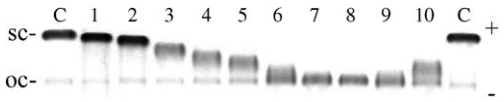

Figure 2. Unwinding of negatively supercoiled pUC19 plasmid DNA by $[Ru_2L_3]^{4+}$. The plasmid was mixed with increasing concentrations of the cylinder in 10 mM Tris·Cl (pH 7.4), incubated for 30 min at 25 °C, and analyzed on 1% agarose gel. Lane C: control (unmodified DNA); lanes 1–10: $r_b = 0.01, 0.02, 0.03, 0.04, 0.05, 0.06, 0.07, 0.08, 0.09, 0.10$, respectively; sc and oc indicate supercoiled and relaxed (nicked) forms of plasmid DNA.

shows an electrophoresis gel in which increasing amounts of $[Ru_2L_3]^{4+}$ have been bound to a mixture of relaxed and negatively supercoiled pUC19 DNA. The unwinding angle is given by $F=-18\sigma/r_b(c)$, where σ is the superhelical density and $r_b(c)$ the number of cylinders bound per nucleotide for which the supercoiled and relaxed forms co-migrate.

The number of cylinders bound per nucleotide was taken to be equal to the mixing ratios, under the assumption that all cylinders present in the sample are completely bound to DNA. This assumption is substantiated by the large apparent binding constant ($5.8\times10^7\,\text{M}^{-1}$) determined for binding of $[Ru_2L_3]^{4+}$ to DNA with a random nucleotide sequence (vide infra; strong association is characterized by $K_{app} > 10^6\,\text{M}^{-1}$).[12] The high value of K_{app} and the low ratio of cylinders to DNA molecules in the experiment implies that at equilibrium almost no free cylinders will be present. Under the present experimental conditions, σ was calculated to be -0.058 on the basis of the data of cisplatin, for which $r_b(c)$ was determined in this study and $F=13°$ was assumed. By using this approach a DNA unwinding angle of $13\pm2°$ was determined for $[Ru_2L_3]^{4+}$. This is less than that induced by iron(II) cylinders ($27\pm3°$,[11]) which is surprising given their very similar sizes and identical charges. This may reflect subtle effects arising from differences in the extent of polarization of the protons on the exterior of these cylinders.

Photocleavage of DNA

Plasmid DNA photocleavage: On irradiation with UVA (365 nm, irradiation at intraligand spectroscopic bands of the cylinder; Figure 3a) or Vis light ($\lambda_{max}\approx580$ nm, irradiation at the metal-to-ligand charge-transfer (MLCT) bands of the cylinder; Figure 3b), $[Ru_2L_3]^{4+}$ induces cleavage of plasmid DNA from the supercoiled form (sc) to the nicked form (oc). The amount of nicked DNA increases with irradiation

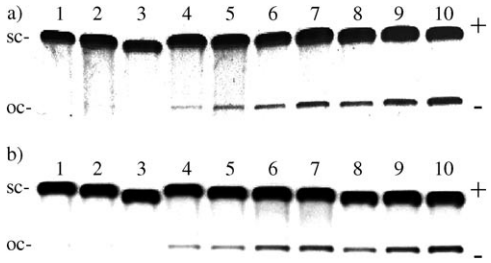

Figure 3. Agarose gels showing photocleavage of pUC19 by $[Ru_2L_3]^{4+}$ on irradiation by UVA (a) and Vis (b) light. Lane 1: DNA in the absence of metal complex incubated in the dark for 80 (a) or 120 min (b); lanes 2 and 3: DNA incubated in the dark for 80 (a) or 120 min (b) in the presence of $[Ru_2L_3]^{4+}$ at 100:1 and 50:1 ratio, respectively; lane 4: DNA in the absence of the cylinder irradiated for 80 min by UVA (a) or for 120 min by Vis (b); lanes 5–7: DNA in the presence of $[Ru_2L_3]^{4+}$ at 100:1 ratio irradiated for 20, 40, and 80 min by UVA (a) or for 30, 60, and 120 min by Vis (b), respectively; lanes 8–10: DNA in the presence of $[Ru_2L_3]^{4+}$ at 50:1 ratio irradiated for 20, 40, and 80 min by UVA (a) or for 30, 60 and 120 min by Vis (b), respectively; sc and oc indicate supercoiled and relaxed (nicked) forms of plasmid DNA.

time and cylinder concentration (Figure 4). The absence of the bands corresponding to the linear form of DNA on the gel indicates that cleavage involves only one strand of DNA at these low cylinder concentrations.

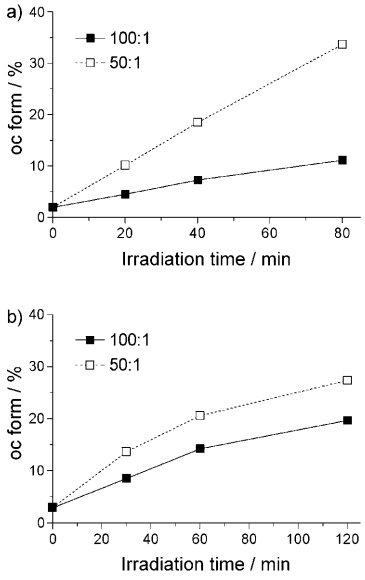

Figure 4. Time dependence of photocleavage activity of $[Ru_2L_3]^{4+}$ on irradiation by UVA (a) and Vis (b) light. ■ and □ represent percentage of nicked DNA in the reaction mixtures containing $[Ru_2L_3]^{4+}$ at 100:1 and 50:1 ratios, respectively.

Mechanism of photocleavage: Ruthenium complexes can induce single-strand DNA breaks on irradiation by different photochemical processes such as singlet-oxygen production, hydroxyl-radical formation, and electron transfer. To determine which process is responsible for photoactivated cleavage of plasmid DNA, photocleavage of pUC19 in the presence of $[Ru_2L_3]^{4+}$ and different inhibitors was examined (Figure 5). Since plasmid cleavage is not inhibited in the presence of hydroxyl radical ($OH^{\bullet}$) scavengers such as mannitol (Figure 5a, lane 3)[13] and DMSO (Figure 5a, lane 4)[14]

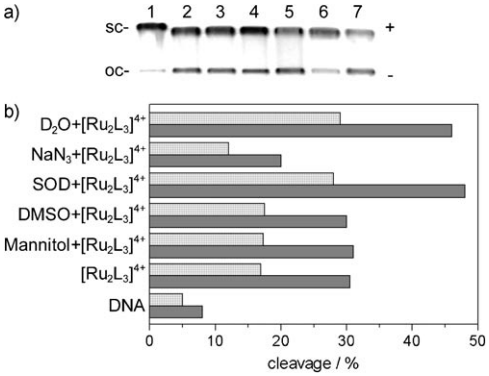

Figure 5. a) Photoactivated cleavage of 200 μM pUC19 in the presence of 2 μM $[Ru_2L_3]^{4+}$ and different inhibitors after irradiation by UVA light for 100 min in 10 μL of 10 mM Tris (pH 7.4). Lane 1: pUC19 in the absence of $[Ru_2L_3]^{4+}$, no inhibitor; lane 2: pUC19 and $[Ru_2L_3]^{4+}$, no inhibitor; lane 3: in the presence of mannitol (100 mM); lane 4: in the presence of DMSO (200 mM); lane 5: in the presence of superoxide dismutase (1000 U mL^{-1}); lane 6: in the presence of sodium azide (10 mM); lane 7: pUC19 and $[Ru_2L_3]^{4+}$ in D_2O (>90% D_2O). b) Bar-graph representation of the effect of inhibitors on the Vis- (light bars) and UVA-activated (dark bars) cleavage activity of $[Ru_2L_3]^{4+}$.

even at high concentrations, the hydroxyl radical is unlikely to be responsible for cleavage. In the presence of superoxide dismutase (SOD), an effective quencher of the superoxide anion radical ($O_2^{\bullet-}$), cleavage was enhanced (Figure 5a, lane 5). Strong enhancement of photonuclease activity by SOD was also observed for $[Ru(bpz)_3]^{2+}$ (bpz = 2,2′-bipyrazyl),[15] and this effect was partly attributed to increased production of singlet oxygen ($^1O_2$) and an electron-transfer process.[16] To test the possibility that photoinduced cleavage involves formation of singlet oxygen, cleavage was carried out in the presence of sodium azide and D_2O. While sodium azide is one of the most effective singlet-oxygen quenchers,[17] $^1O_2$ would be expected to induce more strand scission in D_2O than in H_2O due to its longer lifetime in the former solvent.[18] As shown in Figure 5a (lanes 6 and 7), cleavage of pUC19 by $[Ru_2L_3]^{4+}$ was inhibited in the presence of sodium azide and enhanced in D_2O, that is, $^1O_2$ is likely to be responsible for the cleavage reaction.

Stability of $[Ru_2L_3]^{4+}$ under irradiation by UVA and Vis light was tested under the same experimental conditions, and no decomposition of the cylinder was observed.

Photocleavage of a DNA restriction fragment: The gels in Figure 6a and b show the photocleavage activity of $[Ru_2L_3]^{4+}$ on irradiation by UVA and Vis light, respectively. The main targets of the photocleavage activity on irradiation by both UVA and Vis light are identical and are identified as guanine residues, which are known to be preferentially attacked by singlet oxygen at neutral pH. This is in agreement

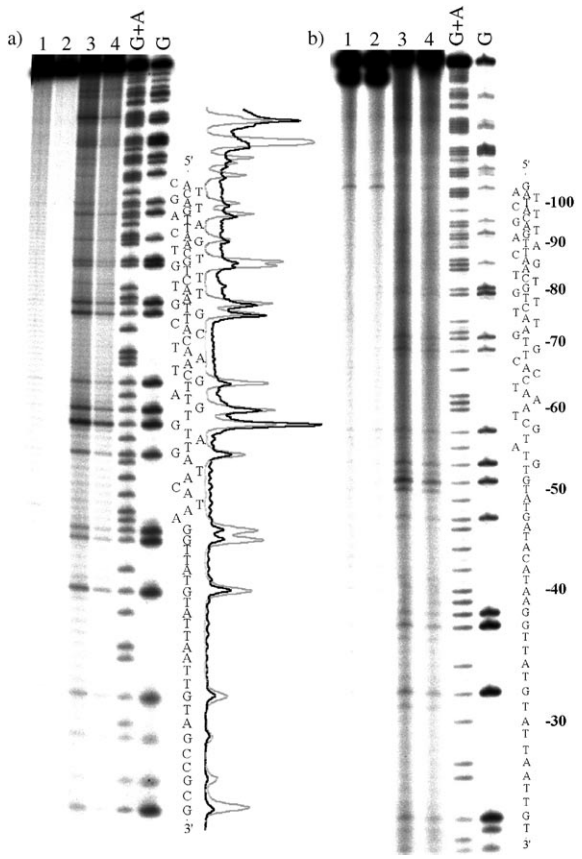

Figure 6. Autoradiograms of 13% polyacrylamide denaturing gels showing photocleavage of 158 bp fragment by $[Ru_2L_3]^{4+}$ on irradiation by UVA (a) and Vis (b) light. Lanes 1, 2: DNA in the absence of $[Ru_2L_3]^{4+}$ irradiated for 4 and 2 h, respectively; lanes 3, 4: DNA in the presence of $[Ru_2L_3]^{4+}$ irradiated for 4 and 2 h, respectively; lanes G+A and G correspond to Maxam–Gilbert G+A and G ladders. The nucleotide sequence of the fragment and the peak areas corresponding to each band are shown on the right side of the gel; gray line, Maxam–Gilbert G ladder, black line, DNA with $[Ru_2L_3]^{4+}$ irradiated for 4 h.

with a photocleavage mechanism involving production of singlet oxygen, as suggested by previous results, possibly in combination with an electron-transfer pathway. The sites of photocleavage on irradiation by UVA light are summarized in Figure 7 and compared with preferential binding sites (vide infra). The sites of photocleavage upon irradiation by Vis light are identical (see Figure 6a and b).

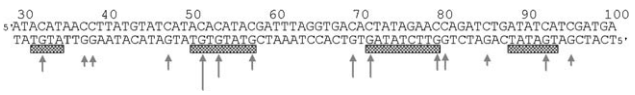

Figure 7. Part of the sequence of 158-mer *Hind*III/*Nde*I fragment of the plasmid pSP73 showing preferential binding (shown as light bars) and photocleavage (indicated by arrows) sites of $[Ru_2L_3]^{4+}$. The binding sites were obtained by shifting the sites of inhibited DNase I cleavage by 2 bp in the 3′ direction.

DNase I footprinting: The 158 base-pair (bp) restriction fragment of pSP73 plasmid identical to that used in the photocleavage experiment (Figures 6 and 7) was also employed for DNase I footprinting. $[Ru_2L_3]^{4+}$ was mixed with the 158 bp restriction fragment at base:cylinder ratios of 6:1, 8:1, 10:1, and 20:1, and then partial cleavage by DNase I was performed. The autoradiogram of the DNA cleavage-inhibition patterns is shown in Figure 8. The extent of DNase I cleavage varies along the fragment sequence. Interestingly, cutting is strongly reduced in several sequences even in the absence of the cylinder (Figure 8, lane 5). In the presence of the cylinder several footprints in the gel demonstrate that $[Ru_2L_3]^{4+}$ is capable of recognizing specific DNA sequences. To obtain further information on the binding specificity of $[Ru_2L_3]^{4+}$, intensities from the gel lanes containing DNA and Ru cylinder at base:cylinder ratios of 8:1 and 10:1 were measured by densitometry. The resulting differential cleavage plots are shown in Figure 9a. Negative values indicate sites of drug protection against DNase I cleavage, and positive values indicate regions of drug-induced enhancement of cleavage. A stretch of DNA of about 70 bp within the 158 bp restriction fragment was sufficiently well resolved that cleavage could be quantified. There are four main short

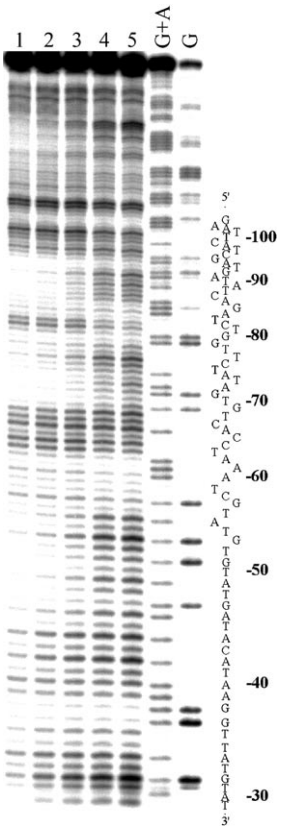

Figure 8. Autoradiogram of DNase I footprint of 3′-end-labeled bottom strand of 158-mer *Hind*III/*Nde*I restriction fragment of plasmid pSP73 in the presence of different concentrations of $[Ru_2L_3]^{4+}$. Lanes 1–4: DNA mixed with $[Ru_2L_3]^{4+}$ at 6:1, 8:1, 10:1 and 20:1 (base:cylinder) ratios, respectively; lane 5: DNA in the absence of cylinder; lanes G+A and G correspond to Maxam–Gilbert G+A and G ladders. The nucleotide sequence of the fragment is shown on the right side of the gel, and numbers refer to the sequence shown in the corresponding differential cleavage plots in Figure 9.

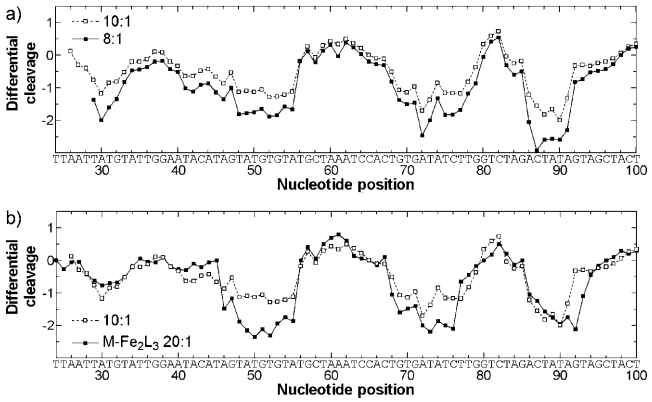

Figure 9. a) Differential cleavage plots for $[Ru_2L_3]^{4+}$-induced differences in susceptibility to DNase I digestion on the bottom strand of 158-mer *Hind*III/*Nde*I fragment of the plasmid pSP73 at 8:1 (full squares) and 10:1 (open squares) base:cylinder ratio. b) Comparison of differential cleavage plots for $[Ru_2L_3]^{4+}$- (open squares) and *M*-$[Fe_2L_3]^{4+}$-induced (full squares) differences in susceptibility to DNase I digestion on the bottom strand of 158-mer *Hind*III/*Nde*I fragment at 10:1 and 20:1 base:cylinder ratio, respectively (data for *M*-$[Fe_2L_3]^{4+}$ obtained under otherwise identical experimental conditions were taken from ref. [11]). Vertical scales are in units of $\ln(f_c)-\ln(f_0)$, where f_c is the fractional cleavage at any bond in the presence of cylinder, and f_0 the fractional cleavage of the same bond in the control, given similar extents of overall digestion. Positive values indicate enhancement, and negative values inhibition.

nucleotide sequences protected by $[Ru_2L_3]^{4+}$, around positions 30, 52, 73, and 89. These sequences consist of regularly alternating purine–pyrimidine nucleotides. Differential cleavage plots of $[Ru_2L_3]^{4+}$ and the *M* enantiomer of $[Fe_2L_3]^{4+}$ (*M*-$[Fe_2L_3]^{4+}$) at base:cylinder ratios of 10:1 and 20:1 are compared in Figure 9b. The Ru and Fe cylinders exhibit very similar patterns of protection and enhancement, but the extent of protection by $[Ru_2L_3]^{4+}$ is somewhat weaker.

To identify the sites of cylinder binding from the sites of inhibited DNase I cleavage, a 3′ shift of about 2–3 base pairs must be considered because of the bias introduced by the nuclease on DNA cleavage.[19,20] The resulting binding sites of $[Ru_2L_3]^{4+}$ are summarized in Figure 7 and compared with photocleavage sites. Notably, the strongest photocleavage sites are situated at the preferential DNA binding sites or in their close proximity.

Conclusion

Metal-based compounds that bind to DNA in a different way to conventional cisplatin and its analogues, particularly those that bind by noncovalent interactions, have considerable potential as anticancer agents with a new spectrum of activity. Modification of DNA secondary structure by binding of molecules of biological significance is an important aspect of recognition by DNA processing proteins in the cell.

The results of the present and earlier[10] work demonstrate that several features of target DNA binding mode of the ruthenium(II) metallosupramolecular cylinder and its iron counterpart are similar, which is not unexpected since both cylinders have essentially the same size and charge. A somewhat surprising result was that $[Ru_2L_3]^{4+}$ unwinds DNA noticeably less than $[Fe_2L_3]^{4+}$. At present, we have no conclusive explanation for this observation. It cannot be excluded that the difference in DNA unwinding is a consequence of very subtle differences in the structures of the two cylinders, consistent with the working hypothesis that the size and shape of the cylinder are crucial for recognition of the purine–pyrimidine tracts to which they preferentially bind (Figure 7 and ref. [11]). Interestingly, $[Ru_2L_3]^{4+}$ unwinds the DNA duplex by 13°, that is, to an extent similar to DNA unwinding by cisplatin,[21] which is also a low molecular mass agent but has a nonintercalative DNA binding mode.

An intriguing feature of DNA binding of $[Ru_2L_3]^{4+}$ is its highly effective DNA-photocleavage ability, a feature not accessible with $[Fe_2L_3]^{4+}$. Mechanistic studies reveal that singlet oxygen ($^1O_2$) may play an important role in photocleavage. In addition, $[Ru_2L_3]^{4+}$ exhibits sequence selectivity in DNA photocleavage with a preference for regularly alternating purine–pyrimidine nucleotides. Agents showing photoinduced cleavage of DNA have significant advantage over their "chemical nuclease" analogues in that other chemical reagents, such as a reducing agent and/or H_2O_2, is not required for their activity. Besides, compounds cleaving DNA on photoactivation usually show localized effects in therapeutic applications and are much less toxic in the absence of light, so that they are particularly useful in photodynamic therapy as specific photoreagents.

The results described here may help to further understand the selectivity and efficiency of DNA recognition and cleavage by dinuclear ruthenium(II) metallosupramolecular cylinders, as well as in developing new useful DNA probes and effective metal-based nucleases. The design of molecules that bind and cleave a selected DNA sequence provides an intriguing opportunity for basic and applied biology. For example, such molecules offer new prospects for controlled manipulation of the genome. In addition, long-wavelength DNA cleavage activity makes these ruthenium(II) metallosupramolecular cylinders potential candidates for further design of molecules suitable for photodynamic therapy applications and as alternatives to the agents already used in clinical photodynamic therapy.

Experimental Section

Starting materials: The synthesis of cylinder $[Ru_2L_3]^{4+}$ (Figure 1) has been described previously.[10] A stock solution of the cylinder was prepared by dissolving the solid PF_6 salt in a small volume of DMSO (less than 10% of the final volume) followed by dilution with water to the final concentration of 1 mM. The concentration was checked by UV/Vis absorbance spectroscopy by using the extinction coefficient $\varepsilon_{485\,nm} = 16870\,M^{-1}\,cm^{-1}$. Ct DNA (42% G+C, mean molecular mass ca. 2×10^7) was prepared and characterized as described previously.[22] Plasmids pUC19 (2686 bp) and pSP73 (2464 bp) were isolated according to standard procedures. *Nde*I and *Hind*III restriction endonucleases were pur-

chased from New England Biolabs (Beverly, MA). [α-^{32}P]-dATP was obtained from MP Biomedicals, LLC (Irvine, CA). The Klenow fragment from DNA polymerase I (exonuclease minus, mutated to remove the 3′-5′ proofreading domain), KF$^-$, was purchased from Takara (Japan). Acrylamide and bis-acrylamide were obtained from Merck KGaA (Darmstadt, Germany), and agarose from FMC BioProducts (Rockland, ME, USA). The Wizard SV and PCR Clean-Up System used to extract and purify the 158 bp DNA fragment (vide infra) was purchased from Promega. EtBr and deuterium oxide (D_2O) were purchased from Merck KGaA, and DNase I was obtained from Roche (Mannheim, Germany). Superoxide dismutase, mannitol, sodium azide, and DMSO were obtained from Sigma-Aldrich (Prague). The 158 bp DNA fragment was prepared by digesting supercoiled pSP73 plasmid with *Nde*I restriction endonuclease and 3′-end-labeled by treatment with KF$^-$ and [α-^{32}P]-dATP. After radioactive labeling, the DNA cleaved with *Nde*I was digested with *Hind*III. The cleavage resulted in 158 and 2306 bp fragments. The 158 bp fragment was purified by electrophoresis on 1% agarose gel and isolated from the gel by Promega Wizard SV Gel cleanup system.

Competition assays: The competition assays were all undertaken with fixed DNA and competitor (EtBr) concentrations and variable helicate concentration. The DNA-EtBr complexes were excited at 546 nm and the fluorescence was measured at 595 nm. Aliquots of a 1 mM stock solution of the cylinders were added to the solution of EtBr and DNA (10 mM Tris pH 7.4, 1 mM ethylenediaminetetraacetic acid (EDTA), 1.3 μM EtBr, and 3.9 μM DNA), and the fluorescence was measured after each addition until it was reduced to 50%. In general the experiments were designed so that the weaker binder was displaced by the stronger one. The apparent binding constants K_{app} for both enantiomers were calculated from $K_{EB}[EB] = K_{app}[drug]$, where [EB] is the concentration of EtBr (1.3 μM), [drug] is the concentration of cylinders at 50% reduction of fluorescence, and K_{EB} is known ($K_{EB} = 1 \times 10^7\,M^{-1}$ for ct DNA).[23]

Unwinding of negatively supercoiled DNA: Unwinding of closed circular supercoiled pUC19 plasmid DNA was assayed by an agarose gel mobility shift assay.[21] The unwinding angle F induced per cylinder bound to DNA was calculated by determination of the cylinder:base ratio at which complete transformation of the supercoiled to the relaxed form of the plasmid was attained. An aliquot of the sample was subjected to electrophoresis on 1% native agarose gel running at 25°C in the dark with Tris-acetate/EDTA (TAE) buffer and the voltage set at 25 V. The gels were then stained with EtBr and photographed with a transilluminator.

Photocleavage experiments

Instrumentation: The light source used in DNA photocleavage experiments was a Photoreactor LZC-ICH2 from Luzchem (Canada) fitted with UVA lamps (4.3 mW cm^{-2}, λ_{max} 365 nm) or with Vis lamps (cool white fluorescent tubes, 400–700 nm with a maximum around 580 nm, 2.8 mW cm^{-2}). The temperature in the light chamber during irradiation was approximately 37°C.

Photocleavage of plasmid pUC19: Photocleavage reactions were carried out in 10 μL volumes contained in 0.65 mL eppendorf tubes. Reaction mixtures containing plasmid DNA pUC19 and $[Ru_2L_3]^{4+}$ at 100:1 and 50:1 (DNA base:cylinder) ratios in 10 mM Tris·HCl (pH 7.4) were irradiated by UVA light for 20, 40, and 80 min or by Vis light for 30, 60, and 90 min. Higher mixing ratios than 50:1 were not used because the cylinder unwinds the supercoiled form of the plasmid and reduces its mobility in the gel, which complicates analysis of the results. All samples were then mixed with loading buffer and loaded onto a 1% agarose gel running at 25°C in the dark with TAE buffer and the voltage set at 25 V. The gels were then stained with EtBr, followed by photography with transilluminator.

Photocleavage of 158 bp DNA fragment: Photocleavage reactions were carried out in 5 μL volumes contained in 0.65 mL eppendorf tubes. The reaction mixtures were prepared with 150 μM ct DNA (0.048 mg/mL, 150 μM related to the phosphorus content) containing 3′-end-labeled restriction fragment and 7.5 μM ruthenium cylinder in 10 mM Tris·HCl (pH 7.4). The samples were irradiated by UVA or Vis light for 2 or 4 h and then analyzed on 13% polyacrylamide (PAA) gel under denaturing conditions.

Stability of $[Ru_2L_3]^{4+}$ on irradiation: Stability of $[Ru_2L_3]^{4+}$ on irradiation by UVA and Vis light was tested in the following way. $[Ru_2L_3]^{4+}$ was diluted in 10 mM Tris·HCl, pH 7.4 to a concentration of 1×10^{-5} M and irradiated for 120 min. Absorbance at 485 nm, which is a maximum of the MLCT band indicative of stability of the cylinder, was measured and compared.

DNase I footprinting: One subclass of footprinting agents that has been developed for determining the sequence-specific binding of small molecules to DNA comprises enzymes such as DNase I.[20] DNase I is an endonuclease that specifically cleaves the O3′–P bond of the phosphodiester backbone of the double-helical DNA substrate. A solution (9 μL) containing 1.11×TKMC buffer (10 mM Tris pH 7.9, 10 mM KCl, 10 mM $MgCl_2$, and 5 mM $CaCl_2$), 3′-end-labeled restriction fragment, 4.5×10^{-4} M ct DNA (144 μg/mL, 4.5×10^{-4} M related to the phosphorus content), and cylinder was incubated for 15 min at 25°C. Cleavage was initiated by addition of 1 μL of 50 μg DNase I per milliliter and allowed to continue for 30 s at room temperature before quenching with 2.5 μL of DNase I stop solution (3 M NH_4OAc and 0.25 M EDTA). Optimal enzyme dilutions were established in preliminary calibration experiments. The sample was then precipitated with ethanol, lyophilized, and resuspended in a formamide loading buffer. DNA cleavage products were resolved by PAA gel electrophoresis under denaturing conditions (13%/8 M urea PAA gel). The autoradiograms were visualized and quantified by using the bioimaging analyzer. Assignment of the cleavage to a particular base was made so that it corresponds to the cleavage of the phosphodiester bond on the 5′ side of that base.

Other physical methods: Absorption spectra were measured with a Varian Cary 4000 UV/Vis spectrophotometer equipped with a thermoelectrically controlled cell holder and quartz cells with a path length of 1 cm. The PAA gels were visualized by using a BAS 2500 Fujifilm bioimaging analyzer, and the radioactivities associated with bands were quantitated with the AIDA image analyzer software (Raytest, Germany).

Acknowledgements

This research was supported by the Academy of Sciences of the Czech Republic (Grants B400040601, IAA400040803, 1QS500040581, KAN200200651, AV0Z50040507, AV0Z50040702), the Ministry of Education of the Czech Republic (MSMT LC06030, ME08017), the Grant Agency of the Ministry of Health of the CR (NR8562-4/2005) and conducted in the context of COST D39 (WGs D39/002/07 and D39/004/06). We thank Gabriel Pascu for cylinder synthesis.

[1] M. J. Clarke, *Coord. Chem. Rev.* **2002**, *232*, 69–93.
[2] M. Galanski, V. B. Arion, M. A. Jakupec, B. K. Keppler, *Curr. Pharm. Des.* **2003**, *9*, 2078–2089.
[3] E. Alessio, G. Mestroni, A. Bergamo, G. Sava, *Curr. Topics Med. Chem.* **2004**, *4*, 1525–1535.
[4] V. Brabec, O. Novakova, *Drug Resist. Updates* **2006**, *9*, 111–122.
[5] C. A. Vock, W. H. Ang, C. Scolaro, A. D. Phillips, L. Lagopoulos, L. Juillerat-Jeanneret, G. Sava, R. Scopelliti, P. J. Dyson, *J. Med. Chem.* **2007**, *50*, 2166–2175.
[6] M. J. Hannon, *Chem. Soc. Rev.* **2007**, *36*, 280–295.
[7] M. J. Hannon, L. J. Childs, *Supramol. Chem.* **2004**, *16*, 7–22.
[8] M. J. Hannon, V. Moreno, M. J. Prieto, E. Moldrheim, E. Sletten, I. Meistermann, C. J. Isaac, K. J. Sanders, A. Rodger, *Angew. Chem.* **2001**, *113*, 903–908; *Angew. Chem. Int. Ed.* **2001**, *40*, 879–884.
[9] A. C. G. Hotze, B. M. Kariuki, M. J. Hannon, *Angew. Chem.* **2006**, *118*, 4957–4960; *Angew. Chem. Int. Ed.* **2006**, *45*, 4839–4842.
[10] G. I. Pascu, A. C. G. Hotze, C. Sanchez-Cano, B. M. Kariuki, M. J. Hannon, *Angew. Chem.* **2007**, *119*, 4452–4456; *Angew. Chem. Int. Ed.* **2007**, *46*, 4374–4378.
[11] J. Malina, M. J. Hannon, V. Brabec, *Nucleic Acids Res.* **2008**, *36*, 3630–3638.

[12] S. Kemp, N. J. Wheate, D. P. Buck, M. Nikac, J. G. Collins, J. R. Aldrich-Wright, *J. Inorg. Biochem.* **2007**, *101*, 1049–1058.
[13] C. C. Cheng, S. E. Rokita, C. J. Burrows, *Angew. Chem.* **1993**, *105*, 290–292; *Angew. Chem. Int. Ed. Engl.* **1993**, *32*, 277–278.
[14] S. A. Lesko, R. J. Lorentzen, P. O. P. Tso, *Biochemistry* **1980**, *19*, 3023–3028.
[15] E. Gicquel, N. Paillous, P. Vicendo, *Chem. Commun.* **1998**, 997–998.
[16] E. Gicquel, N. Paillous, P. Vicendo, *Photochem. Photobiol.* **2000**, *72*, 583–589.
[17] J. R. Kanofsky, *Photochem. Photobiol.* **1991**, *53*, 93–99.
[18] A. U. Khan, *J. Phys. Chem.* **1976**, *80*, 2219–2228.
[19] J. C. Dabrowiak, J. Goodisman in *Quantitative Footprinting Analysis of Drug-DNA Interactions* (Ed.: N. R. Kallenbach), Academic Press, New York, **1989**, pp. 143–174.
[20] K. R. Fox, M. J. Waring in *High-resolution Footprinting Studies of Drug-DNA Complexes Using Chemical and Enzymatic Probes*, (Eds.: J. B. Chaires, M. J. Waring), Academic Press Inc, San Diego/CA, **2001**, pp. 412–430.
[21] M. V. Keck, S. J. Lippard, *J. Am. Chem. Soc.* **1992**, *114*, 3386–3390.
[22] V. Brabec, E. Palecek, *Biophys. Chem.* **1976**, *4*, 76–92.
[23] M. D. Wyatt, B. J. Garbiras, M. K. Haskell, M. Lee, R. L. Souhami, J. A. Hartley, *Anti-Cancer Drug Des.* **1994**, *9*, 511–529.
[24] M. J. Hannon, C. L. Painting, A. Jackson, J. Hamblin, W. Errington, *Chem. Commun.* **1997**, 1807–1808.
[25] J. M. C. A. Kerckhoffs, J. C. Peberdy, I. Meistermann, L. J. Childs, C. J. Isaac, C. R. Pearmund, V. Reudegger, S. Khalid, N. W. Alcock, M. J. Hannon, A. Rodger, *Dalton Trans.* **2007**, 734–742.

Received: July 5, 2008
Published online: October 8, 2008

